Available online at www.sciencedirect.com
ScienceDirect
ELSEVIER
ISPRS Journal of Photogrammetry & Remote Sensing 60 (2006) 375–386
PHOTOGRAMMETRY & REMOTE SENSING
www.elsevier.com/locate/isprsjprs

Studies on DMC geometry

R. Alamús *, W. Kornus, J. Talaya

Institut Cartogràfic de Catalunya, Parc de Montjuïc 08038 Barcelona, Spain

Received 30 September 2005; received in revised form 19 May 2006; accepted 22 May 2006
Available online 7 August 2006

Abstract

Since the ISPRS Congress 2000 in Amsterdam, there are great expectations in matrix-CCD based digital cameras for aerial photogrammetry and mapping applications. During the last two years the number of DMC cameras in the market has raised significantly (32 cameras were sold until March 2006). This paper discusses the DMC accuracy focusing on the role of self-calibration parameters and the assessment of automatic DEM quality. This investigation concluded that under the current status of DMC an appropriate set of self-calibration parameters is necessary in order to achieve theoretical accuracy and precision, which were discussed in early literature.

In the following discussions, the accuracy of the DMC is analyzed comparing its performance in automatic DEM generation to that of an analog camera using a Lidar DEM as reference. Despite the fact that the higher image quality of the DMC should overcome the poorer base-to-height ratio, the presented results did not reach the expected accuracies. However, our current study is not yet conclusive on this topic because the DMC, the analog images and the LIDAR data have not been acquired at the same time.

Keywords: Digital aerial camera; Accuracy; Automatic DEM generation; Self-calibration

1. Introduction

In 2004 the Institut Cartogràfic de Catalunya (ICC) decided to make a commitment to a totally digital mapping workflow. Once the selection phase for a digital camera had been completed, a ZEISS/INTERGRAPH (Z/I) Digital Mapping Camera (DMC) was delivered to the ICC. Following this, the ICC needed to validate, evaluate and find the most suitable strategy to obtain the best possible performance of the DMC. Several blocks were aerotriangulated and studied in detail in order to assess the potential accuracy of the new camera and to investigate the changes on the current photogrammetric models that the new technology may require. This paper focuses mainly on the role of self-calibration parameters and the assessment of quality of automatically generated digital elevation models (DEM) as quality criteria for the DMC.

1.1. DMC camera description

One of the most important DMC features is the capability to simultaneously capture high resolution panchromatic images of 13 824 × 7680 pixels and multispectral images of 3042 × 2048 pixels in 4 bands (red, green, blue and near infrared). The high resolution image is assembled from 4 views taken with inclined cameras

* Corresponding author.
E-mail addresses: ramon.alamus@icc.cat (R. Alamús), wolfgang.kornus@icc.cat (W. Kornus), julia.talaya@icc.cat (J. Talaya).

0924-2716/$ - see front matter
doi:10.1016/j.isprsjprs.2006.05.006

with a focal length of 120 mm, each covering a quarter of the final image (called virtual image). The 4 low resolution multi-spectral images are taken by 4 additional nadir looking cameras with a focal length of 25 mm (one for each color channel) and completely cover the virtual high resolution image (see Hinz, 1999; Zeitler et al., 2002; Dörstel et al., 2003 for details).

2. Data sets

In this section an overview of the different data sets is given, the main features of the blocks used in the study are summarized in Table 1 and Fig. 1.

2.1. Block 'Amposta'

On December 16, 2004 image data of the Amposta block were taken. The block consists of 139 images distributed in 5 parallel and 2 transversal strips, taken at a flight altitude of 800 m above ground level, which corresponds to a ground sampling distance (GSD) of 8 cm. Image orientations were directly measured using a GPS/INS system on board the aircraft. The block contains 7 natural full ground control points (GCP) and 6 natural check points.

The performance of the DMC was assessed and compared to the aerotriangulation results of a block flown over the same area with an analog camera in 2000. The analog block consisted of 69 photographs distributed in 5 parallel strips and 2 transversal strips (exactly the same configuration as the aforementioned DMC block). The block contains 8 natural full ground control points and 1 natural check point.

The 7 full GCP used in the DMC block are a subset of the 8 GCP in the analog block. The 8th point could not be measured in the DMC images. The analog check point is one of the 6 check points used in the DMC block.

2.2. Block 'Rubí'

The data relating to Rubí was acquired on March 8, 2005. The block consists of 426 images distributed in 13 parallel and 3 transversal strips, taken at a flight altitude of 1000 m above ground level, which corresponds to a GSD of 10 cm. 19 natural GCP and 426 orientations derived from GPS/INS data were used to aerotriangulate the block. Moreover, 20 well distributed check points were measured in the images, which belong to the fourth order Geodetic Network of Rubí and have an accuracy of 2 cm in planimetry and 4 cm in altimetry.

2.3. Block '415'

The 415 block covers a rectangular area of 90 km × 20 km, which is the area covered by three 1:50 000 sheets. The block consists of 312 images distributed in 4 parallel and 2 transversal strips, taken at an average altitude of 4500 m above ground level, which corresponds to a GSD of 0.45 m. The block contains 33 full natural GCP, 18 natural check points and 312 orientations derived from GPS/INS data. Furthermore, some areas of the block are covered by a Lidar DEM. In these areas a study of DMC automatic DEM accuracy has been conducted (see Section 3.3).

2.4. Block '419'

The 419 block covers a rectangular area of 30 km × 20 km, which is the area covered by a single 1:50 000 sheet. The block consists of 98 images,

Table 1
Data sets configuration

Block	Amposta	Amposta analog	Rubí	415	419	Caro	546
GSD [m]	0.08	0.08	0.10	0.45	0.47	0.50	0.45
Flying altitude [m]	800	800	1000	4500	4700	5000	4500
End lap [%]	60 (1 strip 80)	60	75	60	60	80	60 (4 strips 80)
Side overlap [%]	25	25	50	25	25	25	25
No. strips/no. cross strips	5/2	5/2	13/3	4/2	4/0	2/0	18/4
No. GPS obs.	139	69	426	312	98	19	363
No. INS obs.	139	0	426	312	98	19	0
No. images	139	69	426	312	98	19	390
No. GCP	7	8	19	33	26	–	42
No. check points	6	1	20	18	22	–	188
Camera	DMC	RC30	DMC	DMC	DMC	DMC	RC30
Focal length [mm]	120.0	150.0	120.0	120.0	120.0	120.0	150.0
Scanning resolution [μm]	–	15	–	–	–	–	15

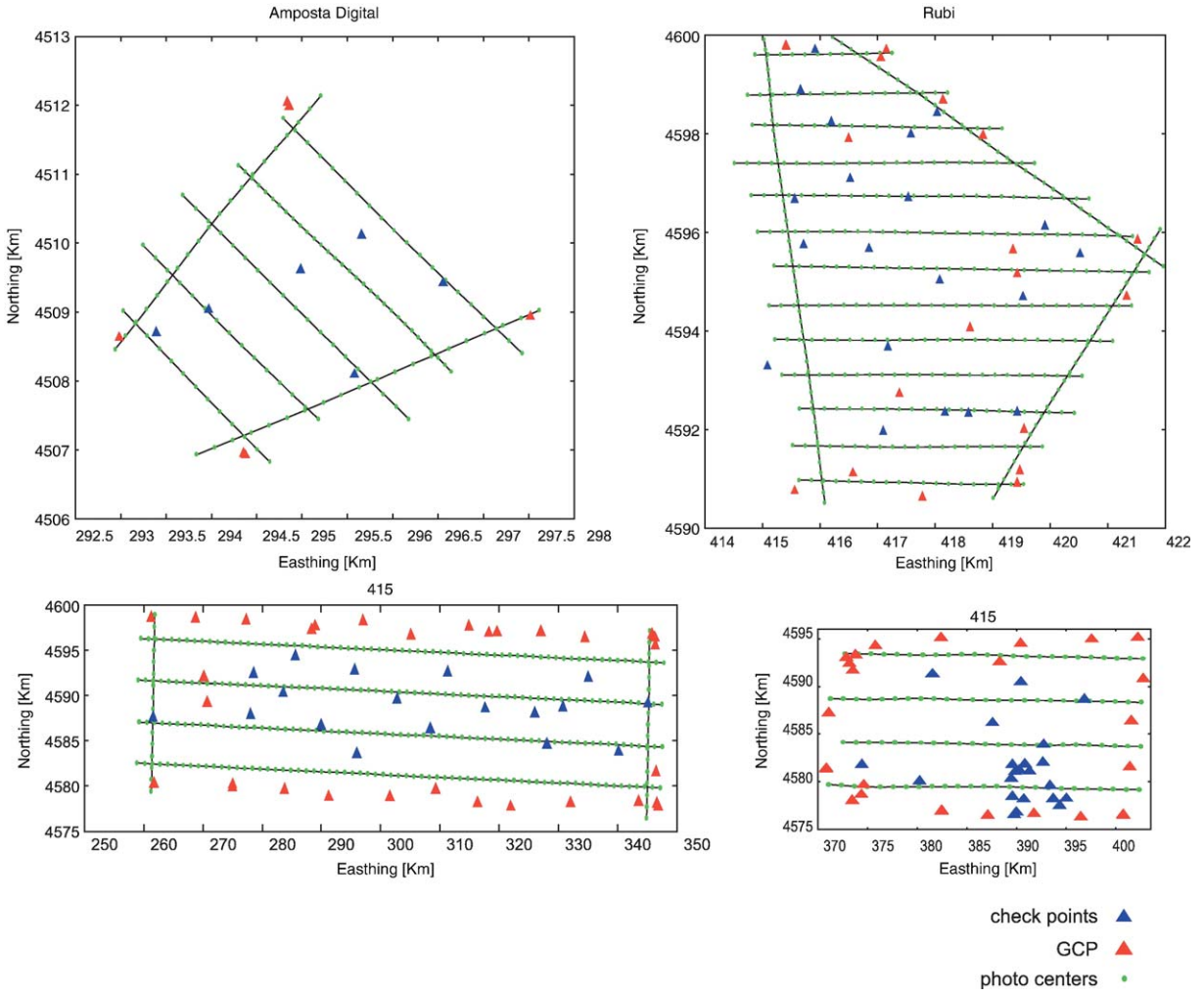

Fig. 1. Sketches of block configuration for blocks Amposta with DMC (Digital, Rubí, 415 and 419).

distributed in 4 parallel strips, taken at an average altitude of 4700 m above ground level, which corresponds to a GSD of 0.47 m. The block contains 26 full natural GCP, 22 natural check points and 98 orientations derived from GPS/INS data.

2.5. Block 'Caro'

The Caro block consists of 19 images, distributed in 2 parallel strips (originally 3, but only 2 of them have been aerotriangulated) taken at an average altitude of 5000 m above the ground, which corresponds to a GSD of 50 cm. The covered terrain is half plain and half mountainous. The block was aerotriangulated with manual point identification. The DMC images were tied to a larger analog block (546, see Section 2.6 below) flown and already aerotriangulated. 19 orientations derived from GPS/INS data were used in the bundle block adjustment.

The main feature of this block is that there is a large difference in height, with up to 1000 m in a single DMC image.

2.6. Block '546'

The 546 block covers an area of 65 km × 40 km close to the coast and was acquired in May 2004 with an analog camera. The block consists of 390 analog images distributed in 18 strips of different lengths and 4 cross strips following the coast line, taken at an average altitude of 4500 m above the ground level, which corresponds approximately to a photo scale 1:30 000. The block contains 42 full natural GCP, 188 natural check points and 363 positions for the projection centers derived from GPS data.

3. Experiments and analysis of results

3.1. Aerotriangulation

The results of DMC aerotriangulation were assessed both in image and in object space in comparison to corresponding aerotriangulations of conventional analog images. In all cases the adjustment was done in UTM projection using the in-house ACX-GeoTex software (Colomina et al., 1992), since all available GCP refer to the UTM coordinate system. In order to increase the robustness of the aerotriangulation the orientations derived from the GPS/INS data were used as observations and adjusted together with the photogrammetric observations.

3.1.1. Pointing accuracy

To assess the pointing accuracy the block Amposta was aerotriangulated three times:

1 using manual photogrammetric observations from the analog RC30 images
2 using manual photogrammetric observations from the DMC images
3 using automatic photogrammetric observations from the DMC images derived by the Match-AT software

In the first case 1188 photogrammetric observations were manually measured in the analog RC30 images after scanning them at 15-μm pixel size. Altogether 217 tie points, 8 full GCP and 1 check point, 69 GPS aerial control points (observations for the projection center positions), one set of linear drift parameters per strip and one set of 12 self-calibration parameters were used in the block adjustment.

In the second case 2757 photogrammetric observations were manually measured in the DMC images, corresponding to 431 tie points, 7 full GCP and 6 check control points. 139 full GPS/IMU aerial control observations (a set of 6 parameters describing the position of the perspective center and the attitude for each image), one set of linear drift parameters per strip and no self-calibration parameters were used in the block adjustment. The photogrammetric model is described in (Baron et al., 2003).

In the third case 17 068 photogrammetric observations of 3068 tie points were automatically derived from the same DMC images by Inpho's Match-AT software using the same control and check point configuration as in case 2. Automatically generated tie points were visually checked focusing in strip and photo connections, if needed, manual edition was carried out. As mentioned above, all 3D data refer to projective UTM coordinates. Since Match-AT works exclusively with Cartesian coordinates, the bundle block adjustments were carried out — as in all the other cases of this study — with the ACX-GeoTex software; i.e. Match-AT was exclusively used for the automatic production of photogrammetric observations. As in the manual case one set of linear drift parameters per strip and no self-calibration parameters were used in the block adjustment.

In all 3 cases the following *a priori* standard deviations were introduced into the adjustment: GPS observations: 10 cm, IMU attitude observations: 20 arc sec, horizontal GCP observations: 5 cm, vertical GCP observations: 6 cm, image observations: 5 μm.

Table 2 shows the root mean squared (RMS) values of all photogrammetric residuals after the bundle block adjustments, which is a reliable measure for the pointing accuracy. The accuracy improves by a factor of 1.3 comparing manual point identification in DMC images to analog images, and even by a factor of 3 if comparing digital image matching in DMC images to manual point identification in analog images.

Table 2
Block Amposta — RMS values of photogrammetric residuals after block adjustment using manually measured points in analog images scanned at 15 μm pixel size (Analog manual), manually measured points in DMC images (DMC manual) and automatically matched points in DMC images (DMC automatic)

	Analog manual		DMC manual		DMC automatic	
	μm	pix.	μm	pix.	μm	pix.
x	4.83	0.32	2.85	0.24	1.23	0.10
y	4.27	0.29	2.35	0.20	1.12	0.09

Table 3
Statistics on the check point accuracies (σ). $\sigma_{predicted}$ is the predicted accuracy according to (Dörstel, 2003)

Block	No. of check points	GSD		Mean	R.M.S	σ	$\sigma_{predicted}$
Amposta	6	8.0 cm	*X*	−0.05 m	0.06 m	0.04 m	0.03 m
			Y	0.01 m	0.02 m	0.02 m	0.03 m
			H	−0.02 m	0.04 m	0.04 m	0.04 m
Rubí	20	10 cm	*X*	−0.00 m	0.04 m	0.04 m	0.04 m
			Y	0.00 m	0.03 m	0.03 m	0.04 m
			H	−0.02 m	0.06 m	0.06 m	0.05 m
415	18	47.0 cm	*X*	−0.09 m	0.25 m	0.24 m	0.20 m
			Y	−0.05 m	0.26 m	0.26 m	0.20 m
			H	0.17 m	0.30 m	0.26 m	0.24 m

3.1.2. 3D point accuracy

The 3D point accuracy is assessed using independent check points. Table 3 shows the statistics of the differences

Table 4
Impact of self-calibration parameters on image point measuring accuracy and point accuracy at the 20 check points of the Rubí block

		No self-calib.		1 set self-calib.		4 set self-calib.	
		Mean	σ	Mean	σ	Mean	σ
Image residuals	x [pix]	0.000	0.146	0.000	0.145	0.000	0.135
	y [pix]	0.000	0.114	0.000	0.113	0.000	0.107
Check point accuracy	X [m]	−0.002	0.031	0.002	0.036	−0.005	0.038
	Y [m]	−0.000	0.047	−0.000	0.036	0.002	0.030
	H [m]	0.000	0.147	0.000	0.149	−0.020	0.062

between the check point coordinates and the aerotriangulation results of the blocks Amposta, Rubí and 415. The results for the blocks Rubí and 415 were generated in the same way as the Amposta block. The *a priori* standard deviations were set to 2 μm for image observations and 10 cm for GPS observations. Table 3 shows the mean, the RMS and the σ values of the coordinate differences at the check points. $\sigma_{predicted}$ relates to theoretical values given in (Dörstel, 2003). It should be noted, that the blocks Rubí and 415 were adjusted with 4 sets of self-calibration parameters, while the Amposta block was calculated without self-calibration (see Section 3.2).

The predicted accuracies of a DMC aerotriangulation are outlined to be 5 μm times the image scale in planimetry and 0.05‰ of the flying altitude in height, which corresponds to 3 cm in planimetry and 4 cm in height for the Amposta block, and 4 cm in planimetry and 5 cm in height for the Rubí block. The respective results in Table 3 are fully consistent in planimetry and a little worse in height. More results are described in Alamús et al. (2005), which demonstrate that analog cameras and the DMC achieve comparable 3D point accuracies in aerotriangulation and also in stereoplotting.

3.2. The role of self-calibration parameters

This section analyzes the potential improvement of the DMC geometry and its temporal stability through the application of self-calibration parameters. ICC's aerotriangulation software allows simultaneous self calibration applying either the standard model of radial and tangential distortions or the 12 parameters proposed by Ebner (Ebner, 1976). The Rubí block was aerotriangulated three times using the same image, control (ground and aerial) and check observations and the same image tie points, generated by Match-AT: Firstly, without self-calibration, secondly, with one set of 12 self-calibration parameters and finally, with four sets of 12 self-calibration parameters. These four sets are related to the four quarters of the DMC image, which are acquired by four different high resolution DMC camera heads. This approach pays tribute to the special DMC design and enables self-calibration of each single camera head. The image coordinates were measured on the virtual image and thereafter split in 4 subsets (1 for each quadrant) based on the image coordinates.

Table 4 and Fig. 2 demonstrate impressively the impact of self-calibration on the photogrammetric object

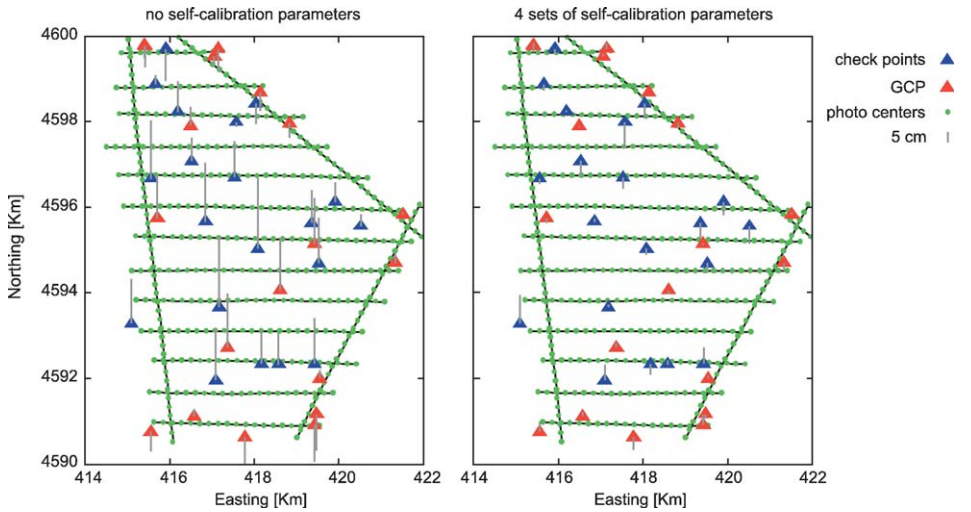

Fig. 2. Rubí block point and height error distribution after triangulation. Left: no self-calibration parameters (similar to one single set — see Table 4). Right: 4 sets of 12 self-calibration parameters.

reconstruction. Table 4 contains the residuals in the image space and the accuracy at the check points for the 3 following cases: Without self-calibration parameters, with a single set of 12 self-calibration parameters and with 4 sets of 12 self-calibration parameters (1 set for each image quadrant). The results show, that a single set of 12 parameters does not significantly improve the statistics of neither the photogrammetric residuals nor the final accuracy at the check points. Nevertheless, 7 of the 12 parameters are estimated significantly with values up to 12 times larger than their standard deviation. 4 sets of 12 self-calibration parameters, which are more appropriate to represent the 4 camera head geometry of the DMC, are capable to remove a systematic height error cutting down height standard deviation from 15 cm to 6 cm on the check points. The image pointing accuracy also improves slightly.

The left part of Fig. 2 shows a systematic distribution of the height residuals with highly positive values in the block center and small or negative values at the borders. In order to evaluate a possible dependence of these height residuals on the block configuration, the Rubí block has been split into two sub-blocks: Rubí-N and Rubí-S. Rubí-N contains the 7 northernmost strips of the Rubí block and the overlapping parts of the transversal strips. Rubí-S contains the 7 southernmost strips of Rubí and the overlapping parts of the transversal strips. Rubí-N and Rubí-S have one strip, 4 GCP and some images of the transversal strips in common.

The three blocks Rubí, Rubí-N and Rubí-S were aerotriangulated without self-calibration and also with 4 sets of 12 self-calibration parameters leaving all other parameters unchanged. Fig. 3 shows the height differences between the tie points resulting from aerotriangulation without self-calibration and with 4 sets of 12 self-calibration parameters. On the left side of Fig. 3 the differences of the complete block are represented, the right side shows the differences of the two sub-blocks. The figure illustrates very well the systematic height error, which is also indicated in Table 4 in case of no or 1 single set of self-calibration parameters and also by the height error distribution at the check points in Fig. 2. If no or only 1 set of self-calibration parameters is applied the point heights are systematically estimated too high. The height error depends on the planimetric position of the point and increases along with its distance from the border of the block. 4 sets of self-calibration parameters reduce this systematic height shift as shown in Table 4 and the right hand side of Fig. 3. This demonstrates clearly that the existing DMC image geometry requires a self-calibration model, which properly takes into account the camera design involving 4 camera heads.

It is known, that the images of the 4 camera heads are fused to a DMC virtual image assuming a predefined mean terrain height for the block (Dörstel et al., 2003). It is also known, that a significant terrain height variation within the block, depending on the flying altitude, introduces geometric errors to that fusion process, which are quantified in (Tang et al., 2000). For the block Rubí (1000 m flying altitude) a height deviation in the order of 100 m produces an error of 0.13 pixel in the image and a height error of 6.4 cm. In Fig. 4 the height error prediction is represented by the blue line. It is noticeable that results at check points using the 4 self-calibration sets of parameters match that error prediction fairly well. However, results using no self-calibration parameters are worse than expected. In this case the predicted errors seam to be magnified by the non-modelled systematic effects of the camera.

Fig. 5 shows the image corrections related to the estimated self-calibration parameters. A single parameter set (left sketch) yields no significant correction in

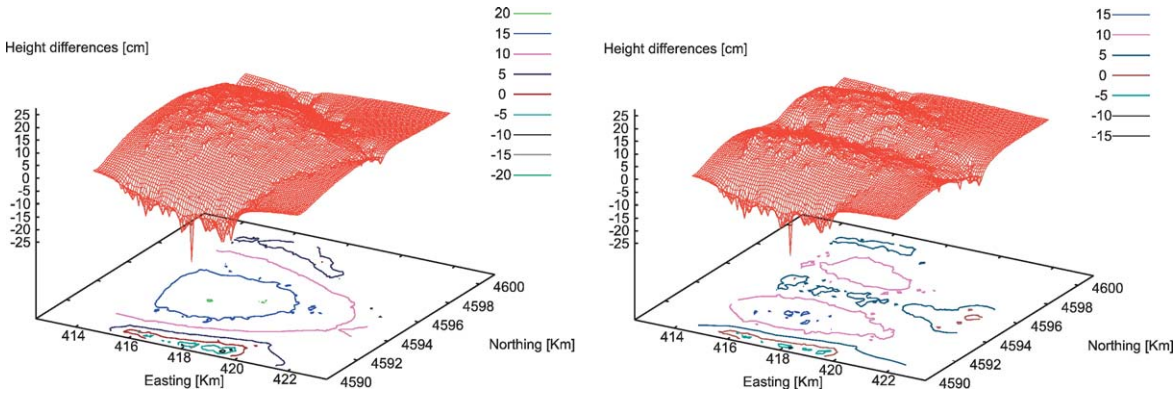

Fig. 3. Height differences between tie points resulting from aerotriangulation without self-calibration and with 4 sets of 12 self-calibration parameters. Left: complete block Rubí. Right: block Rubí split into two sub-blocks.

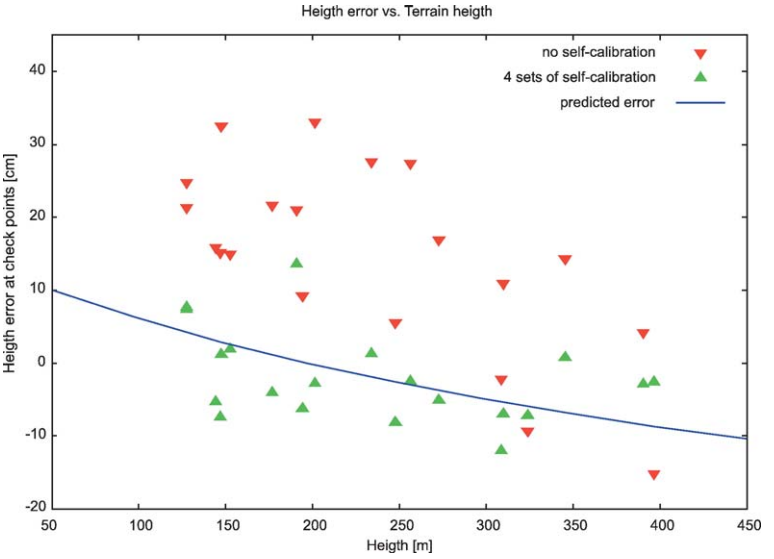

Fig. 4. Height errors at check points plotted against point height. Red: errors without self-calibration. Green: errors using the 4 sets of 12 self-calibration parameters. Blue line: predicted height error according to (Tang et al., 2000). (For interpretation of the references to colour in this figure legend, the reader is referred to the web version of this article.)

image space, as already indicated in Table 4. The 4 sets of parameters (right sketch), however, induce corrections of up to 1 to 1.5 pixels at the edges of the image. The 4 parameter sets and consequently the corrections in the 4 image quarters are significantly different, which suggests that each high resolution head may be affected by different systematic effects.

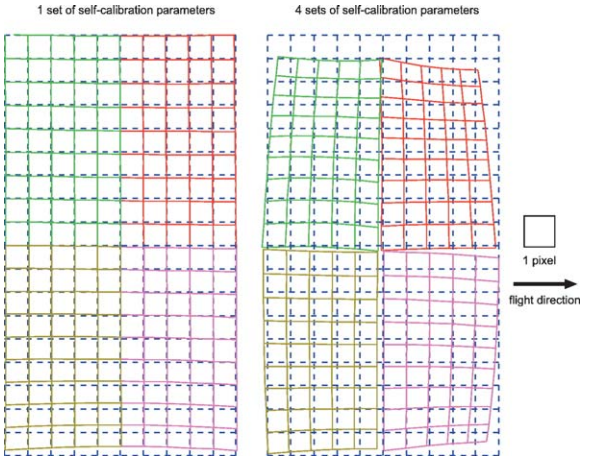

Fig. 5. Image corrections produced by 1 set (left) and 4 sets of self-calibration parameters (right). The blue dashed grid represents the uncorrected DMC image. The corrected grids related to the 4 high-resolution camera heads are painted in different colors. The pixel size at the correction scale is represented on the right. (For interpretation of the references to colour in this figure legend, the reader is referred to the web version of this article.)

The full 4 sets of 12 parameters have also been estimated in the blocks Amposta, 415 and 419 flown at different dates and at different image scales. Fig. 6 shows the respective corrections for each block. All of them show a clear trend in image space, although the parameters vary from block to block.

This section has shown that the commonly used 12 self-calibration parameter set is not capable of providing a significant accuracy improvement in aerotriangulation. Further investigations at the ICC are planned to substitute the used 12 parameter approach by a parameter set, which better represents the 4 camera head-geometry of the DMC in order to achieve the maximum and expected benefit of this new technology.

3.3. Automatic DEM generation

In order to assess the quality of digital elevation models (DEM), in December 2004 the DMC was flown over half plain and half mountainous terrain with height differences of up to 1000 m (block Caro, see above). The DMC images were taken with a GSD of 50 cm and 80% end lap. A larger block of the same area, flown in summer 2004 with a RC30 film camera at photo scale 1:30 000 and 80% end lap, served as a comparison. The film images were scanned with a pixel size of 15 μm. A more detailed description of these flight setups is given in Alamús et al. (2005).

A series of DEMs were automatically produced from the DMC as well as from the RC30 images using

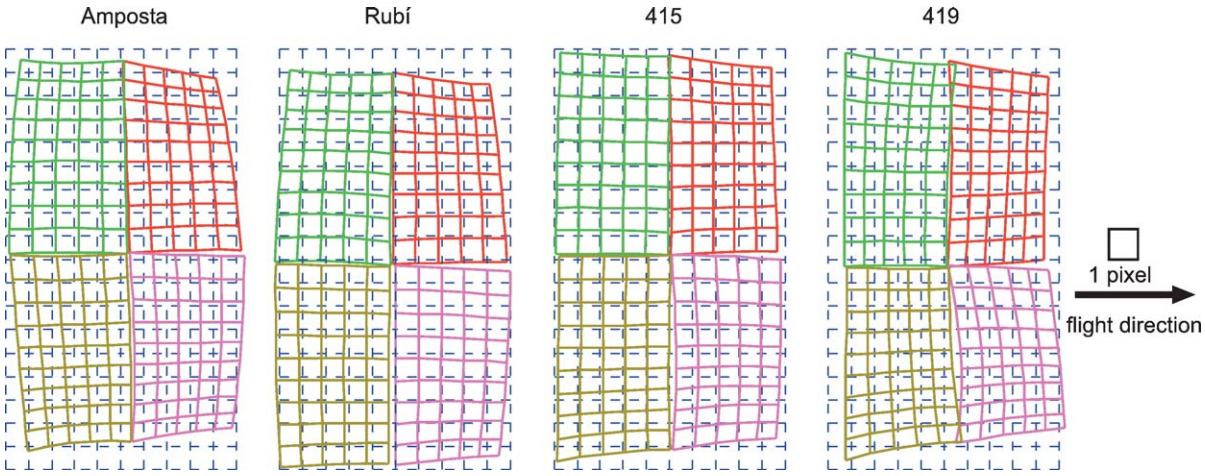

Fig. 6. Image corrections produced by 4 sets of self-calibration parameters for the blocks Amposta, Rubí, 415 and 419 (from left to right).

Intergraph's ISAE software, which applies image matching in object space (Krzystek, 1991). The resulting grid point heights were compared with the ICC's DTM database. Its accuracy of 1.1 m (1σ) is actually too low to analyze all accuracy characteristics of the automatically generated DEM, especially in the flat area, but it is suitable for showing statistical trends, especially in the mountainous area. As results of this comparison the mean height differences, the RMS values and the standard deviations are listed in Table 5, separately for mountainous and flat regions and for the different b/h ratios.

Regarding the mean height differences the DMC points lie significantly above the RC30 points. This systematic effect is not related to vegetation, because it could also be observed on plane surfaces like roads. The actual reason still has to be analyzed. Compared with the RC30 point heights, the DMC points are in general slightly more accurate in the mountainous area and not so accurate in the flat area. Due to the smaller DMC image format in flight direction, the b/h ratio only reaches approximately 50% of that of a conventional frame camera like the RC30, which consequently leads to 50% less height accuracy. According to the manufacturer of the DMC, this accuracy loss is compensated by the higher quality of the digital DMC image and consequently by a higher point measurement accuracy (Dörstel, 2003). We were able to confirm this fact in a series of automatic aerotriangulation runs, which resulted in a σ_0 of approximately 0.1 pixels, compared with approximately 0.3 pixels usually obtained with scanned conventional images. The smaller difference in the viewing direction also improves point matching accuracy and reduces the probability of occlusions in mountainous areas. Probably due to this reason, the accuracy loss of the RC30 between 60% and 80% overlap is less than 50%. The low decrease of 12%–17% in this example may also be a consequence of the low-quality reference data. In the case of the DMC, the results for 60% and 80% end lap are more or less the same and in the flat terrain even 35% worse than the RC30, despite the superior DMC image quality. A possible explanation is that the DMC results are influenced by an up to now unknown effect or the lack of appropriate self-calibration (see Section 3.2), which produces a height error greater than the accuracy change caused by the b/h ratio.

In a new test setup we analyzed a small number of DMC images flown in June 2005 covering the River Segre valley, an area, which had been observed with an OPTECH ALTM 3025 LIDAR system at a mean density of 1 point per m^2 and an accuracy of 1–2 dm only two months before the photo flight. The DMC images were taken from the 415 block, which was aerotriangulated three times: a) without self-calibration; b) with a global set of 12 self-calibration parameters; and c) using the extended model of self-calibration applying one set of 12 self-calibration parameters for each quadrant of the

Table 5
Statistics of height differences [m] between automatically derived DEM grid points and ICC's DTM database

Camera	End lap	b/h	Mountainous area			Flat area		
			Mean	RMS	σ	Mean	RMS	σ
DMC	60%	0.31	1.6	3.8	3.4	1.3	1.9	1.2
	80%	0.15	1.7	3.8	3.3	0.9	1.5	1.3
RC30	60%	0.58	0.5	3.7	3.6	0.1	0.8	0.8
	80%	0.29	0.9	4.3	4.2	0.3	1.0	0.9

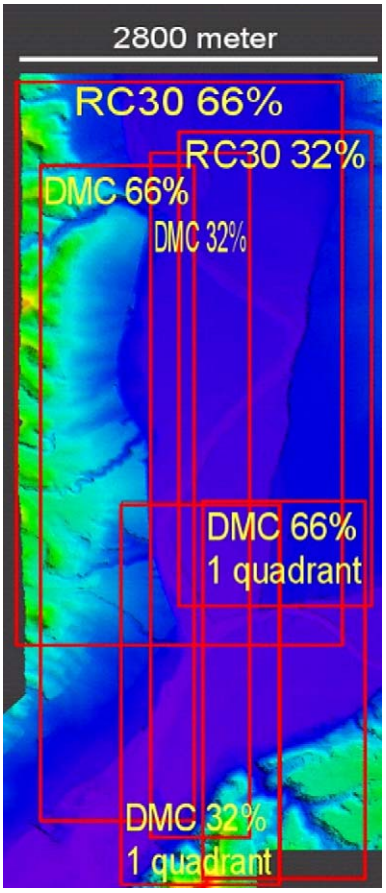

Fig. 7. Location of the investigated models in the River Segre project.

DMC image or each DMC camera head, respectively, as described in Section 3.2. Additionally a larger block exists of the same area, flown in summer 2002 with a RC30 film camera at photo scale 1:22 000 and 60% end lap. The images have been scanned at 15 μm pixel size. A color coded representation of the deduced LIDAR DEM and the location of the individual investigated models are depicted in Fig. 7.

For the accuracy analysis a regular DEM of 5 m grid size for selected models was automatically produced again with the ISAE software. In both cases (RC30 and DMC), the program uses directly the estimated object point coordinates from a well controlled bundle adjustment to compute the exterior orientation for each model. As a result, the software classifies the final grid points in 3 groups: a) regular grid points, b) grid points beyond an internally calculated height accuracy threshold and c) grid points with low redundancy, in this case less than 4 matching points per grid mesh. From the DMC images an average of 87% of the points were matched in class a, 11% in class b and 2% in class c. From the analog images 76% were matched in class a, 13% in class b and 11% in class c. This comparison demonstrates again the high performance of automatic matching with DMC images. Although the 5 m × 5 m grid is covered by less pixels (DMC: 11 × 11 pixels, RC30: 15 × 15 pixels) there are more points matched in class a and significantly less points in class c. For flat terrain ISAE can filter out 3D outliers such as single trees and houses and generate DEM grid points close to the ground. Since the test data is located in flat terrain (River Segre valley), the reference DEM was derived from LIDAR points classified as ground points at 2.5 m grid space. Table 6 shows the statistical results (mean, minimum and maximum height differences, RMS values and standard deviations) of the comparison between the DEM grid points and the LIDAR DEM for different b/h ratios and different self-calibration parameter sets. For a better comparison the last column contains the standard deviations normalized to the DMC GSD.

In the case of the RC30 the height accuracy change between 32% and 66% end lap is 35%. The mean height differences again indicate a significantly positive vertical shift of the DMC points, which will be subject of further investigation. An expected accuracy change for the different b/h ratios is hardly visible and the extended model of 4 × 12 self-calibration parameters does not seem to affect the results at all. A possible explanation for this is

Table 6
Statistics of height differences [m] between automatically derived DEM grid points and the LIDAR reference DEM (last column contains standard deviation normalized to DMC GSD)

Camera	GSD	End lap	b/h	Self-calibration	Number of points	Min	Max	Mean	RMS	σ	σ_{norm}
RC30	0.33	66%	0.49	12 parameters	365 821	−12.40	14.48	0.17	0.53	0.50	0.68
		32%	0.98	12 parameters	182 754	−4.60	7.18	−0.08	0.38	0.37	0.50
DMC	0.45	66%	0.26	None	238 475	−26.66	25.55	0.43	1.13	1.04	1.04
				12 parameters	237 751	−31.68	27.07	0.47	1.09	0.98	0.98
				4 × 12 parameters	238 320	−27.52	24.38	0.42	1.12	1.04	1.04
		32%	0.52	None	156 339	−13.33	17.25	0.40	1.05	0.97	0.97
				12 parameters	157 356	−13.67	18.02	0.46	1.09	0.99	0.99
				4 × 12 parameters	145 209	−9.56	17.68	0.42	1.06	0.98	0.98

Table 7
Statistics of height differences [m] between rigorously calculated object points and the LIDAR reference DEM

Camera	End lap	*b*/*h*	Self-calibration	No. of points	Min	Max	Mean	RMS	σ
DMC	66%	0.26	None	11171	−7.76	16.17	0.56	1.24	1.10
			12 parameters	10956	−7.90	16.22	0.59	1.24	1.09
			4×12 parameters	12597	−7.95	16.26	0.58	1.19	1.04
	32%	0.52	None	6625	−3.73	13.34	0.47	0.87	0.74
			12 parameters	6345	−3.66	13.36	0.50	0.90	0.74
			4×12 parameters	7331	−3.14	13.30	0.40	0.82	0.71

that the ISAE software does not take into account any self-calibration, but calculates an absolute model orientation solely from the estimated ground points by resection. In order to properly analyze the influence of the different self-calibration models, a dense cloud point was generated in image space applying a region growing matching algorithm to just one quadrant of the DMC images, which later was rigorously transformed into object space using the estimated orientation (and self-calibration) parameters. Finally, all object points with *y*-parallaxes less than 0.2 pixels were compared to the LIDAR reference data and their height differences were statistically evaluated (see Table 7).

In these results we can see a height accuracy improvement for the higher *b*/*h* ratio at 32% end lap, which is comparable to the improvement obtained with the RC30 camera in Table 6. For 66% end lap the rigorously calculated points have more or less the same accuracy as the ISAE grid points, while a 32% end lap leads to 30% better accuracies. Comparing the different self-calibration versions a slight improvement in accuracy is visible if the extended 4×12 parameter model is applied. This also demonstrates a potential to improve the geometric modeling of the DMC camera and the processing of the virtual DMC images, respectively.

However, important questions still remain which could not been answered in this study, e.g. why a bigger *b*/*h* ratio is not reflected in an improved ISAE grid point accuracy and why the height accuracies derived from DMC images are always lower compared to the accuracies derived from RC30 images at the same *b*/*h* ratio and comparable image scale, despite the higher image pointing accuracy in DMC images (see Table 2). In order to answer these questions, we will perform a simultaneous flight with DMC, RC30 and LIDAR, which had in fact already been planned for this study, but which unfortunately had to be postponed due to the breakdown of our LIDAR system.

3.4. Effects of GPS weighting

Recent work has focused on the influence of GPS a priori accuracy and the analysis of systematic residuals in image space using the Rubí data set. This investigation was driven by the suspicion that the systematic height errors shown in Fig. 3 might be caused by geometric instabilities of the photogrammetric block.

3.4.1. GPS a priori accuracy

It is well known in photogrammetry that a geometrically stable photogrammetric block requires accurate height control points in the block center or/and accurate aerial (GPS) control points. Otherwise, height deformations will appear in the block center produced by unfavorable error propagation (Ebner, 1975) — similar to the effect observed in the Rubí block (see Fig. 3). The interior of the Rubí block just contains 4 ground control points (see Fig.2), but full GPS/INS data observations are available for each image. Therefore the weak control point configuration has not been considered as a problem.

Nevertheless, additional block adjustments were calculated varying the weight settings for the GPS and the image coordinate observations. Those adjustments have been carried out without any set of self-calibration. The results are summarized in Table 8:

The RMS values of the image residuals show no significant differences in the statistics in image space, but there is a high correlation between the *a priori* accuracy of the GPS and the image observations on one side and the height accuracy in object space on the other side. The height accuracy increases along with the

Table 8
Impact of GPS and image observation *a priori* accuracy on point accuracy at the 20 check points of the Rubí block and image residual statistics without applying self-calibration

A priori accuracy		RMS at check points			Image residuals RMS	
σ_{photo} [μm]	σ_{GPS} [m]	*X* [m]	*Y* [m]	*H* [m]	*x* [μm]	*y* [μm]
6	1.00	0.037	0.024	0.143	1.77	1.38
6	0.10	0.035	0.028	0.060	1.80	1.39
6	0.03	0.034	0.031	0.048	1.84	1.43
2	1.00	0.041	0.026	0.403	1.74	1.36
2	0.10	0.034	0.034	0.190	1.75	1.37
2	0.03	0.034	0.037	0.060	1.80	1.38

weight of the GPS observations, while a high weight of the image observations (2 μm) leads to worse results than a lower weight (6 μm). The best results are obtained with $\sigma_{photo}=6$ μm and $\sigma_{GPS}=0.03$ m. It is very close to the predicted accuracy (Dörstel, 2003), which is 0.04 m in planimetry and 0.05 m in height.

One possible explanation is, that the high DMC image quality providing highly accurate automatic tie point observations (0.1-pixel level, see Table 2) requires highly accurate control information (ground control points and GPS observations) in order to have an effect on the results. In this example the high number of automatic tie points (17 068 observations for 3068 points) also gives an additional weight to the photogrammetric observations in the adjustment and consequently less relative weight to the control information. The fact, that lower weights of the image observations lead to better results than higher weights indicate, that there is still a systematic effect in image space, which negatively influences the results.

3.4.2. Systematic effects in image space

In order to analyze this effect mean photogrammetric residuals were calculated from all images of the block Amposta and also of the block Rubí. In Fig. 7 these mean values are graphically represented in a regular grid of 40×72 nodes. The distance between 2 nodes corresponds to 192 pixels.

Fig. 8 shows that there is a clearly visible systematic distribution of the image residuals with a magnitude of less than 3 μm. The distribution for block Amposta flown in December 2004 is quite similar to the distribution for block Rubí flown in March 2005, which demonstrates clearly, that systematic influences are persistent in time and therefore can be removed by postprocessing using calibrated correction values.

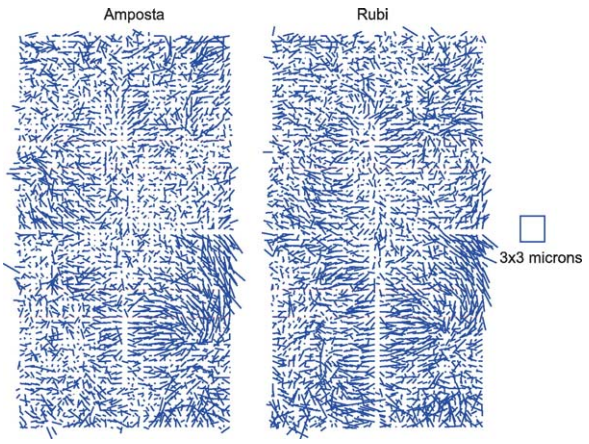

Fig. 8. Averaged image residuals in Amposta (left) and Rubí (right). Average residuals have been computed in the nodes of a grid of 40×72 nodes equally distributed in the virtual DMC image space.

4. Conclusions

The initial tests showed that the point measurement accuracy improves dramatically when using digital DMC images while the 3D point accuracy is comparable with that of analog cameras. The results obtained are in agreement with the predicted DMC theoretical accuracies.

Statistically significant self-calibration parameters have been obtained when considering 4 independent sets of self-calibration parameters (one for each image quadrant) in the block adjustments. This approach is able to model the DMC systematic errors detected in the adjustments, allowing them to reach the theoretical accuracies and precision forecasted in the first published papers about DMC features, capabilities and accuracy. In particular, after applying these sets of parameters the height accuracy agrees with the theoretical analysis described in (Tang et al., 2000). Nevertheless, it has been proven that a persistent systematic distortion in the virtual image is present and, apparently, miscalibrated. Further investigation should be carried out to understand the source of the systematic patterns and to derive more rigorous models to overcome them.

Current investigations suggest that the high quality of the DMC images, at least when used with automatic aerotriangulation methods, could require a highly accurate control (GPS and ground) in order to overcome systematic errors in height when appropriate self-calibration parameters cannot be estimated.

With respect to DEM accuracy, it would appear that the DMC overcomes the handicap of the smaller b/h ratio with its higher point accuracy in mountainous areas and the handicap is barely noticeable in flat areas. Unfortunately, the data sets under study do not allow any final conclusion to be reached. Further work should complete the studies on DEM generation by using data from a simultaneous flight with LIDAR and DMC sensors.

Acknowledgement

We gratefully thank the Institute of Photogrammetry and GeoInformation at the University of Hannover (Prof. C. Heipke) for providing us with the region growing matching software and especially Dr. K. Jacobsen for his very helpful comments and discussions on the image distortion effects.

References

Alamús, R., Kornus, W., Palà, V., Pérez, F., Arbiol, R., Bonet, R., Costa, J., Hernández, J., Marimon, J., Ortiz, M.A., Palma, E., Pla, M., Racero, S., Talaya, J., 2005. Validation process of the ICC digital camera. International Archives of Photogrammetry. Remote Sensing and Spatial Information Sciences (Part I/W3) — on CD-ROM 36.

Baron, A., Kornus, W., Talaya, J., 2003. ICC experiences on inertial/GPS sensor orientation. ISPRS WG I/5 Workshop "Theory, Technology and Realities of Inertial/GPS Sensor Orientation". 22–23rd September 2003, Castelldefels (Spain) — on CD-ROM.

Colomina, I., Navarro, J., Termens, A., 1992. GeoTeX: a general point determination system. International Archives of Photogrammetry and Remote Sensing 29, 656–664 (Part B2).

Dörstel, C., 2003. DMC — practical experiences and photogrammetric system performance. In: Photogrammetric Week 2003 Fritsch D. (Ed.), September 2003 Sttutgart (Germany), Wichmann Verlag, Heidelberg, pp. 59–65.

Dörstel, C., Jacobsen, K., Stallmann, D., 2003. DMC — photogrammetric accuracy–calibration aspects and generation of synthetic DMC images. In: Grün, A., Kahmen, H. (Eds.), Optical 3-D Measurement Techniques VI. Institut for Geodesy and Photogrammetry, vol. I. ETH, Zürich, pp. 74–88.

Ebner, H., 1975. Automatische Kompensation Systematischer Fehler bei der Blockausgleichung mit Unabhängigen Modellen. In: Vorträge des Lehrgangs Numerische Photogrammetrie (III). Esslingen 1975. Institut für Photogrammetrie, Universität Stuttgart Schriftenreihe, Heft 1, 1976.

Ebner, H., 1976. Self-calibrating block adjustment. International Archives of Photogrammetry and Remote Sensing 21 (Part 3).

Hinz, A., 1999. The Z/I digital aerial camera system. Proceedings of the 47th Photogrammetric Week. 1999, Stuttgart (Germany). Wichmann Verlag, Heidelberg, pp. 109–115.

Krzystek, P., 1991. Fully automatic measurement of digital elevation models. Proceedings of the 43th Photogrammetric Week. 1991, Stuttgart (Germany). Wichmann Verlag, Heidelberg, pp. 203–214.

Tang, L., Dörstel, C., Jacobsen, K., Heipke, C., Hinz, A., 2000. Geometric accuracy potential of the digital modular camera. International Archives of Photogrammetry and Remote Sensing 33, 1051–1057 (Part B4/3).

Zeitler, W., Dörstel, C., Jacobsen, K., 2002. Geometric calibration of the DMC: method and results. International Archives of Photogrammetry, Remote Sensing and Spatial Information Sciences 34, 324–333 (Part 3b).